Chem. Pap.
DOI 10.1007/s11696-017-0161-4

ORIGINAL PAPER

Hydrogenation of diacetyl over composite-supported egg-shell noble metal catalysts

N. Carrara[1,2] · J. M. Badano[1,3] · F. Coloma-Pascual[4] · C. Vera[1,3] · M. Quiroga[1,3]

Received: 31 October 2016 / Accepted: 11 March 2017

Abstract Two composite supports with a mixed inorganic–organic structure were synthesized: BTAl and UTAl. Hydrophilic–hydrophobic dual properties of the supports were suitable for preparing egg-shell-supported metal catalysts for selective hydrogenation reactions. The catalysts were characterized by ICP, XRD, OM, TEM, EPMA, XPS and TGA. Their mechanical resistance was assessed. Activity and selectivity were tested with the hydrogenation of 2,3-butanedione (diacetyl) to 3-hydroxy-2-butanoneacetoin (acetoin). The same order of increasing metal particle size was found for the two tested supports: Pt < Ru < Pd. The XPS analysis showed that the metal/composite catalysts reduced in H2 at 503 K had two kinds of active sites: reduced (Me°) and electron-deficient (Me^{+}). It was rationalized that the hydrogen bond cleavage was performed on the Me° active sites, while reactant adsorption occurred on the Me^{+} sites. The differences in activity and selectivity between the composite catalysts were attributed to electronic effects on the different metals and to different adsorptive properties of the different polymers. The high selectivity to acetoin was attributed to the preferential adsorption of diacetyl as compared to the adsorption of acetoin. The BTAl catalysts were slightly more active and selective than the UTAl ones. This was attributed to electronic effects caused by remnant organic groups on the composite supports (urethane or biphenyl on UTAl or BTAl, respectively). Pd-BTAl was the most active and selective catalyst, a fact related to electronic effects of both palladium and the support.

Keywords Composite support · Egg-shell catalysts · Selective hydrogenation · Metal effect

✉ J. M. Badano
jbadano@fiq.unl.edu.ar

[1] INCAPE-CONICET, Instituto de Investigaciones en Catálisis y Petroquímica, Ruta 168 Km 0, S3000AOJ, Santa Fe, Argentina

[2] Universidad Tecnológica Nacional, Facultad Regional Santa Fe, Lavaise 610, S3004EWB, Santa Fe, Argentina

[3] Facultad de IngenieríaQuímica (UNL), Santiago del Estero 2829, S3000AOJ, Santa Fe, Argentina

[4] Servicios Técnicos de Investigación, Facultad de Ciencias, Universidad de Alicante, Apartado 99, 03080 Alicante, Spain

Introduction

Catalytic hydrogenation reactions are widely used for the production of fine chemicals and specialties (Osawa et al. 2000). An important subset of these reactions involves the transformation of vicinal diketones. The hydrogenation of (α,β-diketones) is schematized as A → B → C, where A: α,β-diketone, B: α-hydroxyketone and C: α,β-alkanediol. In these reactions the control of the selectivity to α-hydroxyketones is difficult because the hydrogenation to the α,β-alkanediol is usually favored or because the hydrogenolysis to monoketones is also favored (Hayakawa et al. 2000). α-Hydroxyketones are widely used as intermediates for other products because its dual functionality allows their use in several reactions (Hayakawa et al. 2000). For example α-hydroxyketones can be transformed into vic-diols or α-aminoketones (Nakamura et al. 1996). Vic-diol compounds can be used as solvents or intermediates for the synthesis of other products (Grafje et al. 2012).

Hydrogenation of (α,β-diketones) can be performed by homogeneous (Hayakawa et al. 2000), heterogeneous (Augustine 1997) or enzymatic catalysis(Nakamura et al.

Published online: 18 March 2017

1996). The reduction of 1,2-, 1,3- and 1,4-diketones can be performed by Clemmensen reduction (Di Vona et al. 1990), zinc being used as the reducing agent in acid media. Hayakawa et al. (Hayakawa et al. 2000) carried out the reduction of a 1,2-diketone using TiI_4 in dichloromethane as reducing agent, obtaining excellent yields (up to 92%) in the synthesis of benzoin from diphenylglyoxal. Zuo et al. (2001) studied the catalytic hydrogenation of 2,3-butanedione over Pt catalysts modified by other metal complexes, finding that the modifiers had influence on both the reaction activity and selectivity. Toukoniitty et al. (2003) studied the solvent effect in the hydrogenation of phenyl-1,2-propanedione. Gertosio et al. (1999) studied the effect of the metal function in the hydrogenation of a steroid with α-diketone functionality towards the α-hydroxyketone (11-oxo,12b-OH) and obtained 100% yield.

Metal-based egg-shell catalysts are very important in industry. A low contact time between reactives and active sites and a better surface heat transfer are some of the good qualities of these types of catalysts. Because of these properties, they are appropriate for strongly exothermal reactions where the intraparticle mass and heat diffusion can decrease the catalyst selectivity or lifetime, e.g. by coke formation (Lin and Chou 1994). Iglesia et al. (1995) studied the preparation of cobalt egg-shell catalysts for Fischer–Tropsch synthesis, and found that their use increased the reaction rate and C_5 selectivity. Badano et al. (2010a) developed new "composite" supports with a dual phase matrix (organic–inorganic) with hydrophilic–hydrophobic nature and found that they could be advantageously used for the preparation of egg-shell metal catalysts (Carrara et al. 2014, 2015). This kind of support was used to prepare low loaded palladium catalysts for the selective hydrogenation of styrene and terminal and non-terminal alkynes.

In the present work two composite supports were used to prepare different Pt, Pd and Ru noble metal catalysts. They were evaluated in the reaction test of selective hydrogenation of a diketone, 2,3-butanedione (diacetyl, DC), as shown in Fig. 1. The intermediate product is 3-hydroxy-2-butanone (acetoin, AC) and the total hydrogenated product is 2,3-butanediol (BD). The intermediate product, AC, is used in the flavor and fragrances industry, while the totally hydrogenated BD is used in the cosmetic industry as humectant or in the production of polymers such as Vulkollan (Grafje et al. 2012). The objectives of this work are to evaluate the effect of the metallic active phase and the composite support on the activity and selectivity during the hydrogenation of 2,3-butanedione.

Experimental

Catalyst preparation

The composite supports BTAl and UTAl were prepared following the technique described by Badano et al. (2010a). A fine powder of γ-Al_2O_3 as inorganic phase was added to a mixture of bifunctional monomers as organic phase and benzoyl peroxide as polymerization initiator. The monomers used were bisphenol A glycerolatedimethacrylate (BGMA), triethylene glycol dimethacrylate (TEG) and diurethanedimethacrylate (UDMA). A BTAl composite support was prepared using BGMA and TEG. UTAl was prepared using with UDMA and TEG. The mixture were placed in an oven at 373 K for 1 h to activate the initiator and start the polymerization and stored at 353 K for 12 h. The supports were cut into cylinders of 1.2 mm diameter and 3 mm length. Finally the support was pretreated in N_2 flow at 503 K for 2 h.

Metals were added to the supports by impregnation to incipient wetness using an aqueous acidic solution of the metal precursor ($PdCl_2$, $RuCl_3$ or H_2PtCl_6) at pH 1. The concentration of these solutions was adjusted to obtain a metal loading on the catalysts of ca. 1 wt%. The catalysts were named 1Pd-BTAl, 1Pd-UTAl, 1Pt-BTAl, 1Pt-UTAl, 1Ru-BTAl and 1Ru-UTAl. After the impregnation the catalysts were ground to a size of 35–80 mesh and stored in desiccator for further use. Prior to the reaction the catalysts were activated in H_2 flow at 503 K for 60 min.

Characterization techniques

The catalysts were characterized by inductively coupled plasma ICP-OES, X-ray diffraction, X-ray photoelectron spectroscopy (XPS), microscopy (optical and TEM), electron probe micro-analysis (EPMA), and thermogravimetric analysis (TGA and SDTA). The composite supports were also subjected to mechanical tests for assessing their compression and attrition resistance.

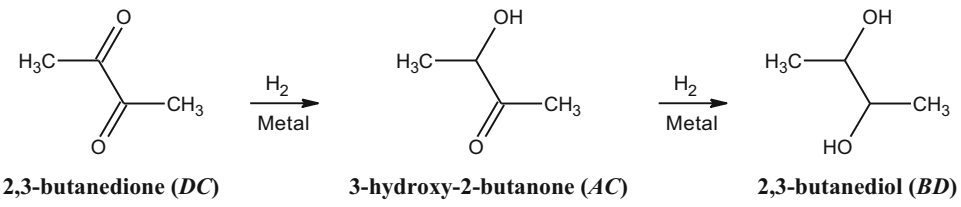

2,3-butanedione (*DC*) 3-hydroxy-2-butanone (*AC*) 2,3-butanediol (*BD*)

Fig. 1 Reaction scheme for 2,3-butanedione hydrogenation

The metal content of the catalysts was obtained by digesting the sample and then analyzing the liquors in a Perkin Elmer Optima 2100DV ICP-OES equipment.

X-ray diffractograms were obtained in a Shimadzu XD-1 equipment, using Cu Kα radiation ($\lambda = 1.5405$ Å) filtered with Ni. The $2\theta = 20$–$80°$ range was scanned at a rate of $1° \text{ min}^{-1}$. The samples were prepared by milling the material to a fine powder and reducing it in hydrogen.

Optical micrographs were obtained with a Mitsubishi Microwatcher VS-30H Microscope and a Sony Color Video Printer. The samples used were either pellets or powders with 35–80 meshes size.

For the transmission electron microscopy (TEM) the samples were milled and then dispersed in a 50% v/v ethanol:water solution for further analysis. The measurements were performed in a JEOL JEM-1200 EXII equipment.

XPS measurements were carried out with a MultitechUniSpecs equipment. Measurements were done using a VG-MicrotechMultilab equipment, with a MgK (*hv* 1253.6 eV) radiation source and a pass energy of 50 eV. The XPS system analysis pressure was kept at 5×10^{-7} Pa. Samples were reduced ex situ 1 h with H_2 at 503 K and treated in situ for 10 min in the instrument chamber before recording the spectrum. A careful deconvolution of the spectra was made. The areas of the peaks were estimated by calculating the integral of each peak after subtracting a Shirley background and fitting the experimental peak to a combination of Lorentzian/Gaussian lines of 30–70% proportions. The reference binding energy (BE) was the Al 2*p* peak at 74.4 eV.

Thermo gravimetric analysis (TGA) traces were also obtained. The experiments were carried out in a TA Instruments 2950 apparatus. The catalyst samples (about 10 mg) were heated in a 40 mL min^{-1} air flow from room temperature up to 1173 K at a heating rate of 5 K min^{-1}.

Values of the axial and radial mechanical resistance of the pellets were obtained in an Instron Marks Universal Rehearsals equipment. A rate of 1 mm min^{-1} was used. The reported values were the result of the averaging of ten experiments with different samples. The attrition resistance measurements were performed following the ASTM D 4058-92 norm.

Catalytic activity tests

The catalytic performance of the prepared catalysts was tested in a semi-continuous stainless steel batch reactor (slurry), equipped with a magnetic stirrer and with PTFE-coated internals. The catalysts were ground to a fine powder to eliminate mass transfer limitations. The reactor was charged with a solution of 2,3-butanedione (diacetyl, DC) in isopropanol (initial concentration of diacetyl, $C°_{DC} = 0.188$ M), and a certain mass of the activated catalyst. Then the reactor was closed. Before the reaction, the reactor was pressurized with N_2 up to 5 bar and purged 3 times, to eliminate oxygen traces. The reaction begun with the hydrogen entrance into the system. During the reaction the stirring speed was maintained at 1200 rpm, the pressure was kept constant at 20 bar and the temperature at 353 K. Runs were carried out in triplicates with an experimental error of 3%. Reactants and products were analyzed by gas chromatography in a Shimadzu 2014 equipment with a flame ionization detector and a 30 m J&W INNOWax 19091N-213 (cross-linked polyethylene glycol phase) capillary column.

Results and discussion

Characterization

X-ray diffraction (XRD)

The X-ray diffractograms of the supports and catalysts are shown in Fig. 2a, b (1 M-UTAl and 1 M-BTAl catalysts). In these figures the signals of the γ-alumina phase and the metal phase have been marked with symbols.

The diffractograms of the support UTAl and the UTAl-based catalysts can be seen in Fig. 2a. In all cases the typical signals of γ-Al_2O_3 are present at 33°, 37.7°, 46°, 62° and 67° (Huang et al. 2008). The organic portion of the composite is amorphous, so it does not produce diffraction peaks. In Fig. 2a the intense peak at $2\theta = 39.9°$ of the 1Pd-UTAl catalyst was attributed to the (111) plane of metallic Pd° (Ngamsom et al. 2004). In the 1Pt-UTAl catalyst a small peak appears at $2\theta = 39.7°$, which would correspond to the (111) plane of Pt° (Onoe et al. 2007; Shul et al. 1986; Huang et al. 2006). In the case of the 1Ru-UTAl catalyst no peaks are observed, possibly due to the proximity of the (101) main plane of Ru to a strong support peak at $2\theta = 43.3°$, as reported by other authors (Marshall et al. 2005). Anyway small particles of Ru on the catalyst that could be detected by TEM are well below the detection limit of the X-ray diffraction technique.

In Fig. 2b diffractograms of the BTAl support and its catalysts can be seen. The main features and conclusions that can be drawn are the same as those previously discussed for the BTAl catalysts.

Optical microscopy (OM), electron probe micro-analysis (EPMA) and transmission electron microscopy (TEM)

The results of optical microscopy (OM) of the composites and the supported 1% Pt, 1% Pd and 1% Ru catalysts are shown in Fig. 3a–h. The images were obtained with

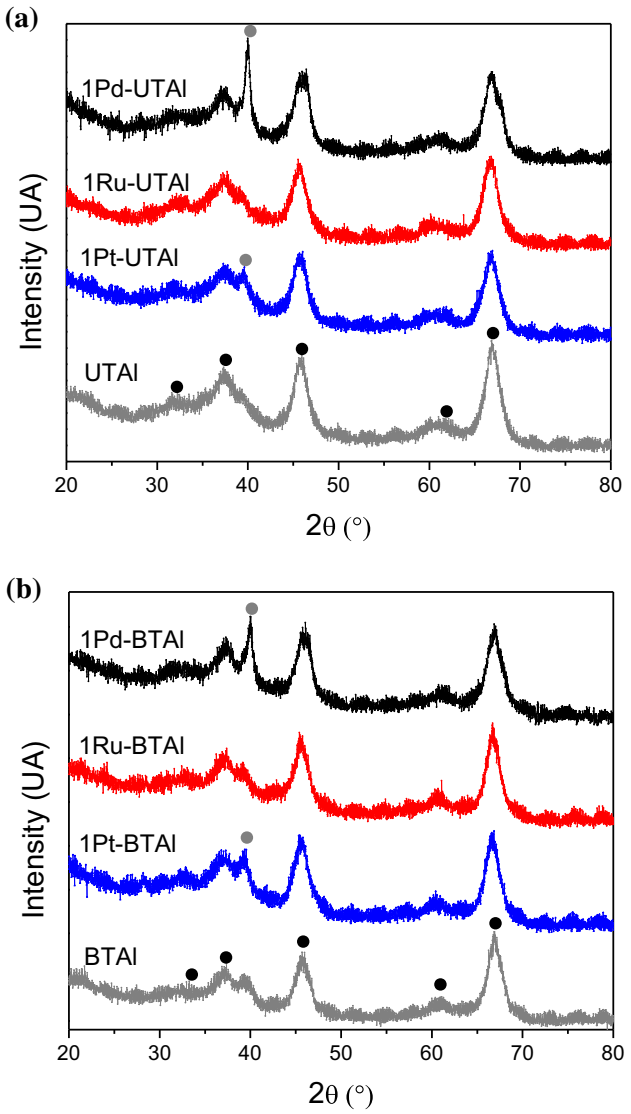

Fig. 2 X-ray diffractograms. **a** UTAL support and catalysts. **b** BTAl support and catalysts

pelletized catalysts. The metal phase of the catalyst can be seen in the periphery, indicating an egg-shell metal distribution. The polymeric phase of the support matrix can be appreciated in dark color, while the inorganic phase is seen in light color. In all the photos the organic phase is seen surrounding the alumina particles.

Values of the Pd/Al mass ratio inside the catalyst pellets were obtained by means of EPMA. The catalyst pellets were coated with a layer of carbon by vacuum deposition. The scanning speed was 0.02 mm min^{-1} and the acceleration voltage of the electron beam was 20 kV. Results of EPMA are presented in Fig. 4. Plots of metal concentration as a function of the pellet radius are presented, for the 1Pd-BTAl and 1Pd-UTAl catalysts. As it can be seen, both catalysts exhibit egg-shell distributions of the metal phase, the metal concentration decreases drastically towards the center of the pellet.

Electronic transmission micrographs of the BTAl and UTAl supports and catalysts can be seen in Fig. 5. In Fig. 5a, b the inorganic phase of the BTAl and UTAl composite support can be distinguished as the region in gray shade while the organic phase has a light color or it is white. In Fig. 5c–h the Pt, Ru and Pd phases can be distinguished as the dark-colored zone surrounding the alumina phase. It must be noted that in these micrographs no metal phase is observed on the polymeric phase.

Optical and transmission electron microscopy images corroborate that the main features of the impregnation mechanism of the metal precursor are dictated by the hydrophilic–hydrophobic nature of the alumina–polymer matrix. In the preparation procedure an acidic aqueous solution of the precursor metal was used. This solution would wet the hydrophilic particles (alumina) located more near the external surface. The hydrophobic polymeric material would act as a barrier preventing the impregnation of the inner particle core by the aqueous solution.

Figure 6 shows the distribution of particle diameters on each composite catalyst. The values of the average volume-surface diameter (D_{VA}) as calculated using Eq. (1) are given in Table 1.

$$D_{VA} = \frac{\sum n_i \cdot d_i^3}{\sum n_i \cdot d_i^2}. \quad (1)$$

Taking this average volume-surface diameter for each catalyst, the dispersion (D) on the surface of the catalysts was estimated following a procedure explained by Badano et al. (2010b). The estimated D values are also given in Table 1.

Metal content and X-ray photoelectronic spectroscopy

Results of metal content are presented in Table 1. The content of each composite catalyst was between 0.86 and 1.1%. The metal content, as measured by ICP, gives information on the effectiveness of the incipient wetness technique for impregnating catalysts with a precise desired amount of metal. The results indicate that the error of the technique was ±14%.

The Pd $3d_{5/2}$, Pt $4d_{5/2}$ and Ru $3p_{3/2}$ XPS spectra of the Me-composite catalysts, previously reduced in H_2 at 503 K, are shown in Fig. 7. The spectra had a peak at about 198.5 eV that corresponds to Cl $2p_{3/2}$. This would be due to chloride species that were not eliminated during the thermal treatment (Badano et al. 2010b; NIST 2016). From the position, maximum intensity and area of the peaks of the XPS spectra, binding energies and relative concentration of surface metal species were determined. From the analysis

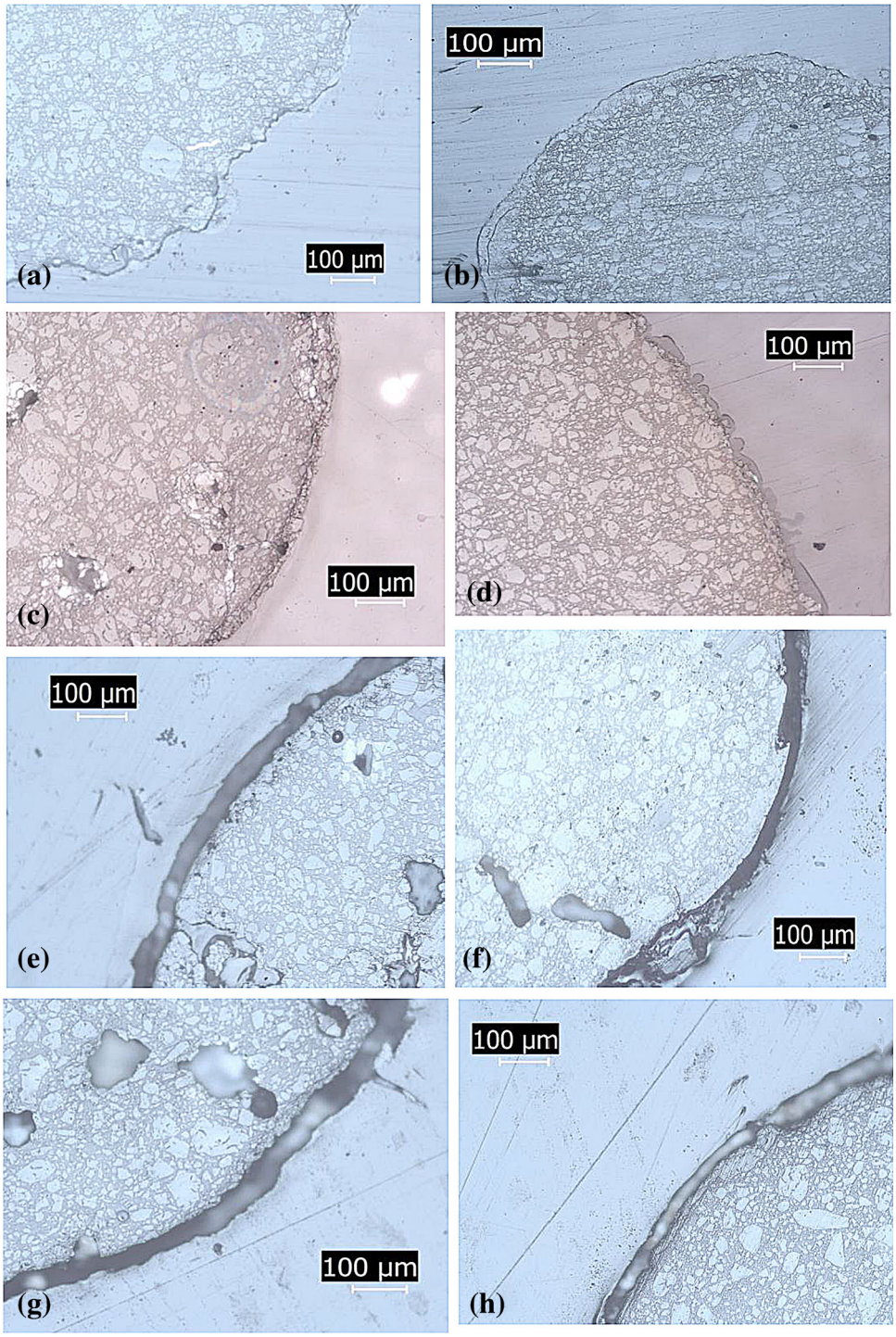

Fig. 3 Optical microscopy images of different metal catalysts. **a** 1Pt-BTAl, **b** 1Pt-UTAl, **c** 1Ru-BTAl, **d** 1Ru-UTAl, **e** 1Pd-BTAl, **f** 1Pd-UTAl, **g** BTAl, **h** UTAl

of the chlorine signals also the Cl/Al atomic ratio was determined. Binding energies and atomic ratios can be found in Table 1.

The XPS results of the Pt-composite catalysts can be seen in Table 1. For these samples the low-intensity Pt $4d_{5/2}$ signals were studied and not the stronger Pt $4f_{7/2}$ ones because the latter are overlapped with the signals due to the alumina component of the support, Al 2*p*. In both samples (1Pt-BTAl and 1Pt-UTAl) two peaks were detected, one at 313.5 eV and another at 315.5 eV that can be assigned to Pt° and to electron-deficient Pt^{n+} ($n \rightarrow 2$) chloride species (Serrano-Ruiz et al. 2006; La Surface 2016). In both cases, Pt° is present in a concentration of ca. 50% indicating that the reduction treatment was insufficient or that a strong interaction with the support was present and precluded an easy reduction. The

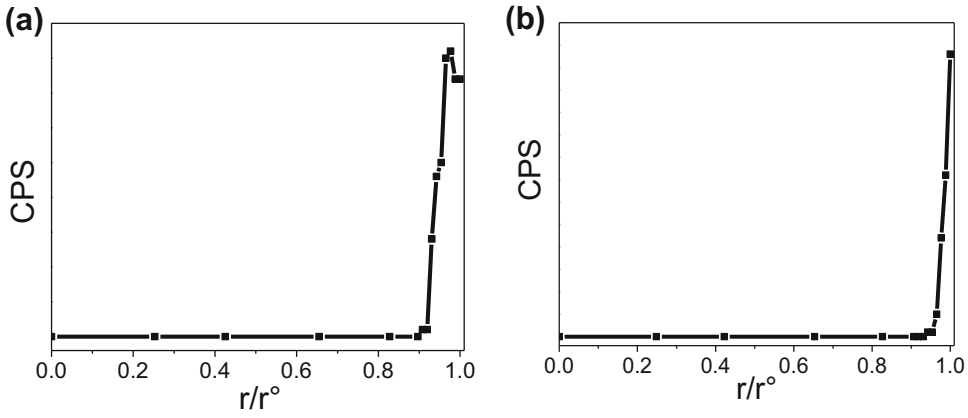

Fig. 4 Metal radial concentration pattern of the Pd catalysts as obtained by EPMA. r° is the external pellet radio. **a** 1Pd-BTAl, **b** 1Pd-UTAl. (Badano et al. 2010a)

BTAl catalysts had a higher surface chlorine content than the UTAl-supported ones.

With respect to the XPS results of the Ru/composite catalysts, the region analyzed was that of the Ru $3p_{3/2}$ binding energy, because the Ru3d band overlaps with the C1s band. In both samples two Ru species could be detected, one with binding energy at about 461.0 ± 0.3 eV and another species with binding energy at about 463.3 eV. According to the literature reports they would be due to Ru° and to $Ru^{\delta+}$ ($\delta \rightarrow 3$) chloride species (Badano et al. 2010b; NIST 2016). The amount of Ru° on both composites is very similar. With respect to the Cl/Al ratio the greater residual chlorine content is found on the BTAl support. Ruthenium catalysts had the highest Cl/Al surface atomic ratios which is consistent with the higher oxidation state of ruthenium.

Two peaks due to Pd were detected in the spectra of the catalysts, one at about 335.3 ± 0.2 eV and another at 336.7 ± 0.3 eV, attributed to Pd° and Pd^{n+} ($n \rightarrow 2$). The signal of oxidized Pd would be related to the presence of chloride species (Badano et al. 2010b; NIST 2016). In both catalysts the dominant surface species was metallic Pd, a desired feature for efficient hydrogenation catalysts. With respect to the Pd oxidized species, it could be formed by non-reduced Pd atoms, stabilized by neighboring chlorine atoms that were not eliminated during the reduction treatment at 503 K (Badano et al. 2010b). The Cl/Al ratios of the Pd/composite catalysts shown in Table 1 indicate the presence of surface chlorine, not eliminated during the thermal pretreatment of the catalysts. The composite Pd-BTAl had a higher content of superficial Cl^- than Pd-UTAl.

Thermal gravimetry

The thermal gravimetry tests give information on the thermal stability of the supports and catalysts and they allow determining the appropriate temperatures for thermal pretreatment and reaction. The obtained results are plotted in Fig. 8a–d.

Figure 8a shows the thermal degradation pattern of the UTAl support and the UTAl catalysts. It can be seen that these materials begin to lose weight noticeably at about 523 K. The presence of metal in the catalysts contributes to speed up the decomposition of the organic matrix of the support. The order of stability is: UTAl > 1Ru-UTAl > 1Pd-UTAl > 1Pt-UTAl. For all samples at the end of the test a residue remains of about 50% the initial mass. This residue corresponds to the inorganic portion of the support, γ-Al_2O_3.

Figure 8c shows the thermal gravimetry traces of the BTAl support and catalysts. In all cases it can be seen that the samples are stable up to 523 K. At temperatures higher than this value a rapid decomposition of the organic part of the sample occurs. As it was the case with the UTAl support and catalyst these materials are more rapidly decomposed in the presence of the noble metal. The order of thermal stability for the samples was: BTAl > 1Ru-BTAl ≈ 1Pd-BTAl > 1Pt-BTAl. In all cases the final residue of about 50% the original mass, corresponded to the inorganic portion of the support.

Figure 8b, d shows the differential thermal analysis (SDTA) traces of the UTAl and BTAl supports and catalysts. In these tests the temperature difference between the sample and a reference is registered, thus allowing to detect if the process is endothermal or exothermal. The traces of the supports show three distinctive zones:

- From room temperature to 523 K the process is endothermal.
- The 523–773 K zone is exothermal, correlating with the decomposition of the organic matrix.
- Above 773 K no temperature differences between the sample and the reference were recorded. This coincides with the evolution at constant mass of the inorganic phase.

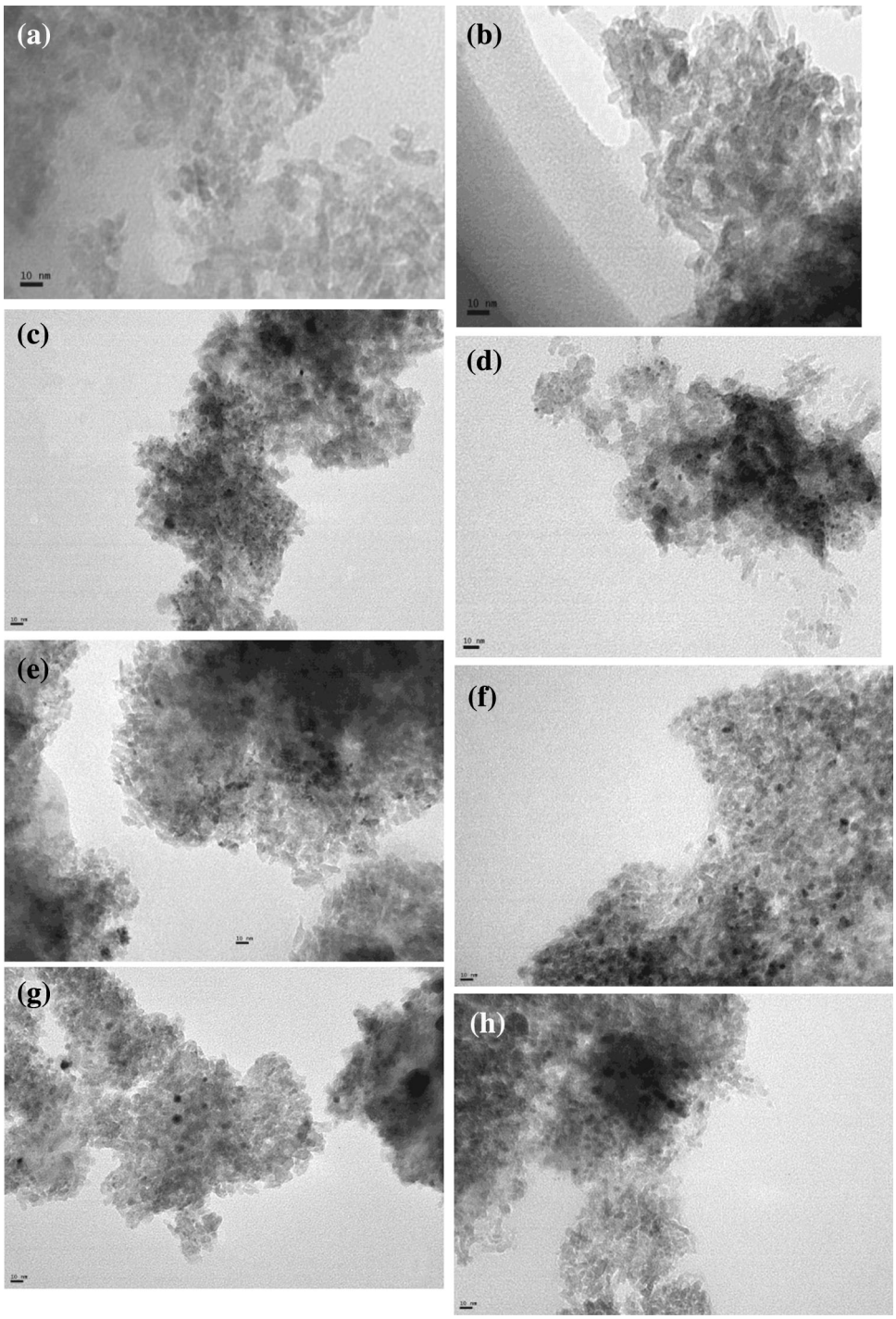

Fig. 5 TEM images of some catalyst fragments. **a** BTAl, **b** UTAl, **c**1Pt-BTAl, **d** 1Pt-UTAl, **e** 1Ru-BTAl, **f** 1Ru-UTAl, **g** 1Pd-BTAl, **h** 1Pd-UTAl

Decomposition of the organic matrix in the 523–773 K range would correspond to the occurrence of cracking, depolymerization and oxidation reactions. Andrzejewska et al. (1993) have reported that during the thermal decomposition of highly interlinked polymers a competition occurs between the phenomena of depolymerization and decomposition.

Figure 8b, d shows a shift of the SDTA traces to lower temperatures. The effect is more important for the UTAl support and would indicate that the noble metals promote the decomposition of the polymeric phase and that Pt has the strongest promoting effect.

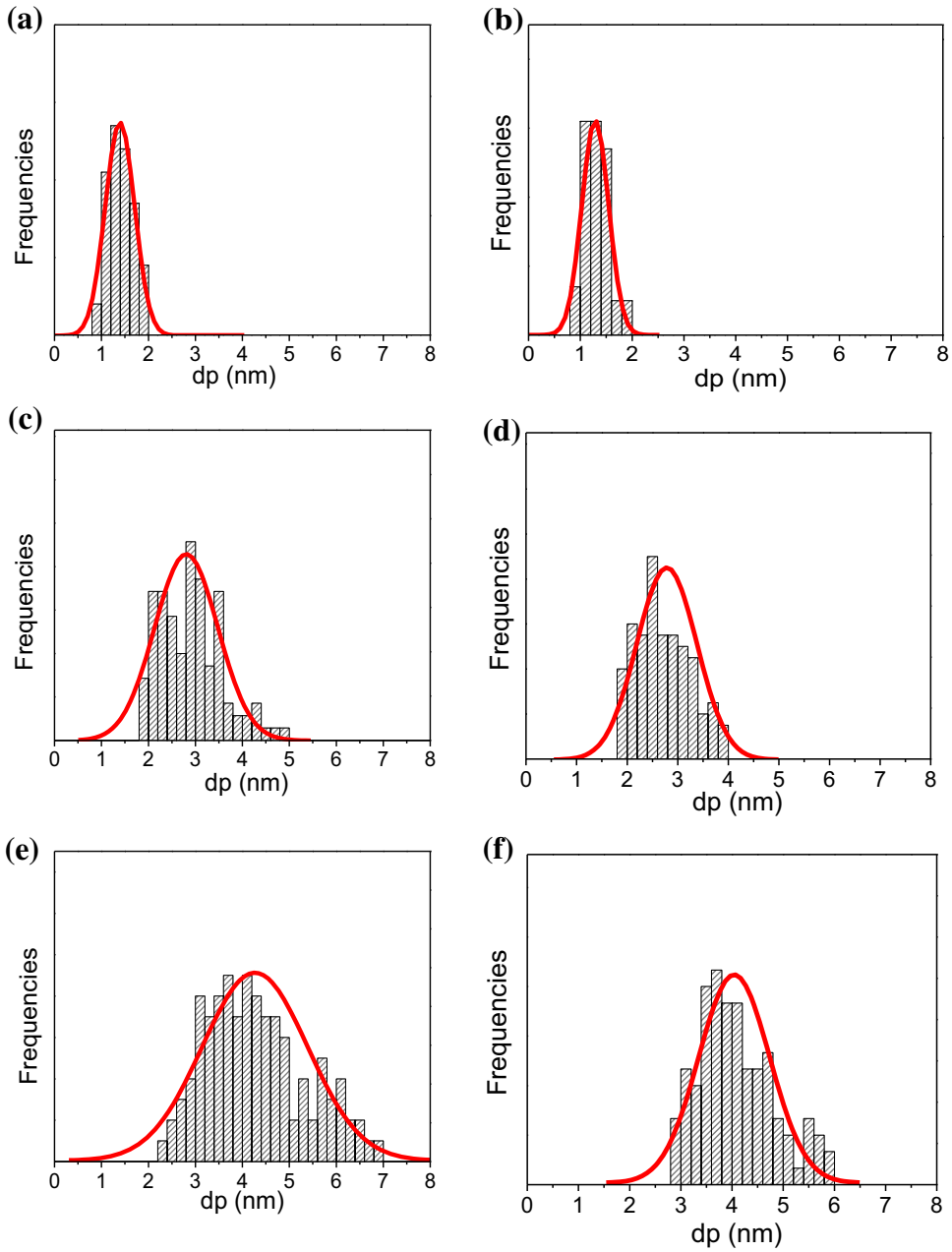

Fig. 6 Metal particle size distribution of catalysts observed with TEM. **a** 1Pt-BTAl, **b** 1Pt-UTAl, **c** 1Ru-BTAl, **d** 1Ru-UTAl, **e** 1Pd-BTAl and **f** 1Pd-UTAl

Mechanical properties of the supports

Figure 9 shows the results of resistance to diametral compression (RDC), resistance to longitudinal compression (RLC), and resistance to attrition of the tested commercial supports (carbon, alumina) and the composite supports (UTAl, BTAl). Attrition resistance tests were made in accordance with ASTM D4058–92 norm (1800 turns). One special test had a longer duration (18,000 turns).

As it can be seen in Fig. 9a–d the results of the mechanical properties indicate that the commercial supports have a lower resistance than the composite supports, UTAl being the most resistant. The order of compression resistance was UTAl > BTAl > α-Al_2O_3 > γ-Al_2O_3 > carbon, and the order of attrition resistance (long test) was UTAl > BTAl > γ-Al_2O_3 > α-Al_2O_3 > carbon. The greater resistance of the composite supports can be explained by their preparation method. The polymer covers the inorganic particles and prevents its attrition.

Parent et al. (2011) developed ceramic catalysts that had better attrition resistance due to the presence of metal oxides in their structure (e.g. NiO, MgO, K_2O), achieving up to 0.3% $^{w}/_{w}$ attrition loss in a 48-h test in a laboratory-scale fluidized-bed reactor system. However, their preparation procedure was somewhat cumbersome and involved long thermal treatments and high temperatures. Scherzer

Table 1 Metal content as determined by ICP, metal particle size and dispersion, and XPS results

Catalyst	Metal loading (wt%)	Metal dispersion (%)	Average particle diameter (nm)	XPS	
				BE and atomic ratio	Cl/Al atomic ratio ($^{at}/_{at}$)
1Pt-BTAl	0.86	75.50	1.4	313.6 eV (55%)	0.0142
				315.5 eV (45%)	
1Pt-UTAl	0.90	80.89	1.3	313.5 eV (48%)	0.0134
				315.5 eV (52%)	
1Ru-BTAl	0.95	40.43	3.3	461.3 eV (76%)	0.0551
				463.3 eV (24%)	
1Ru-UTAl	0.90	44.48	3.0	460.8 eV (77%)	0.0263
				463.2 eV (23%)	
1Pd-BTAl	1.10	22.86	4.3	335.5 eV (75%)	0.0131
				337.0 eV (25%)	
1Pd-UTAl	1.00	24.89	4.2	335.0 eV (80%)	0.0088
				336.4 eV (20%)	

et al. (1991) developed high attrition resistant cracking catalysts for FCC that were prepared by spray drying of an aqueous solution of molecular sieves, kaolin (clay) or silica and aluminum chloride hydroxide. The best catalyst presented an attrition loss lower than 1% $^{w}/_{w}$ and was formed by 20% zeolite (CREY), 15% silica (NALCO 2326), 15% alumina and 50% kaolin.

Not only the composite supports have many advantages, but their preparation is simple and they do not need any thermal treatments. However, composite supports have a maximum temperature limit of 503 K, their use being restricted to reactions performed at temperatures lower than this limit.

Catalytic activity results

All catalysts were active in the reaction of hydrogenation of 2,3-butanedione (DC). The only reaction products found were 3-hydroxy-2-butanone (AC) and butanediol (BD). No traces of reaction products coming from the total hydrogenation of one or two carbons (2-butanone, 2-butanol or butane) were detected. This can be explained by a rapid desorption of the products of partial hydrogenation and their lower affinity for the surface, their subsequent hydrogenolysis or oligomerization being precluded (Rylander 1985).

The results of the reaction tests are shown in Fig. 10a, c in terms of total conversion of 2,3-butanedione (X_{DC}) as a function of reaction time for all catalysts, and in Fig. 10b, d in terms of selectivity to AC as a function of time. No induction period can be seen in the activity plots.

Figure 10a shows plots of total conversion of 2,3-butanedione (X_{BD}) for BTAl catalysts and Fig. 10b shows their selectivity to 3-hydroxy-2-butanone (S_{AC}) as a function of time. Figure 10c shows plots of total conversion of 2,3-butanedione (X_{BD}) for UTAl catalysts and Fig. 10d shows their selectivity to 3-hydroxy-2-butanone (S_{AC}) as a function of time.

Table 2 shows values of total conversions of DC and selectivities to 3-hydroxy-2-butanone at 60 and 120 min of reaction time. The turn over frequencies (TOF) were calculated using values of metal dispersion calculated from the TEM average particle size, and the initial reaction rates, estimated from the plots of Fig. 10a, c by extrapolation to zero reaction time.

The analysis of the results of Fig. 10 and Table 2 indicates that the active metal phase more appropriate for obtaining the intermediate product in high yield is Pd, while the metal that provides the highest selectivity to 2,3-butanediol is Pt. The order of selectivity to 3-hydroxy-2-butanone is: 1Pd-BTAl > 1Pd-UTAl $\gg$ 1Ru-UTAl $\geq$ 1Ru-BTAl > 1Pt-BTAl $\gg$ 1Pt-UTAl. Meanwhile, the order of activity is: 1Pd-BTAl $\gg$ 1Pt-BTAl > 1Pt-UTAl $\gg$ 1Ru-BTAl > 1Pd-UTAl > 1Ru-UTAl.

Gertosio et al. (1999) studied the metal effect in the hydrogenation of a steroid with diketonic functionality and obtained similar results. They obtained the following activity order as based on the initial volumetric reaction rate: Pt > Ru > Pd. The Pd catalyst had an induction period much higher than the rest of catalyst. However, total conversion over the Pd catalyst was got, once the induction period was reached. If values of the reaction rate order are compared almost identical values can be seen for the system of this work and the system of Gertosio et al. (1999).

The high selectivity to the intermediate product could be the results of several factors:

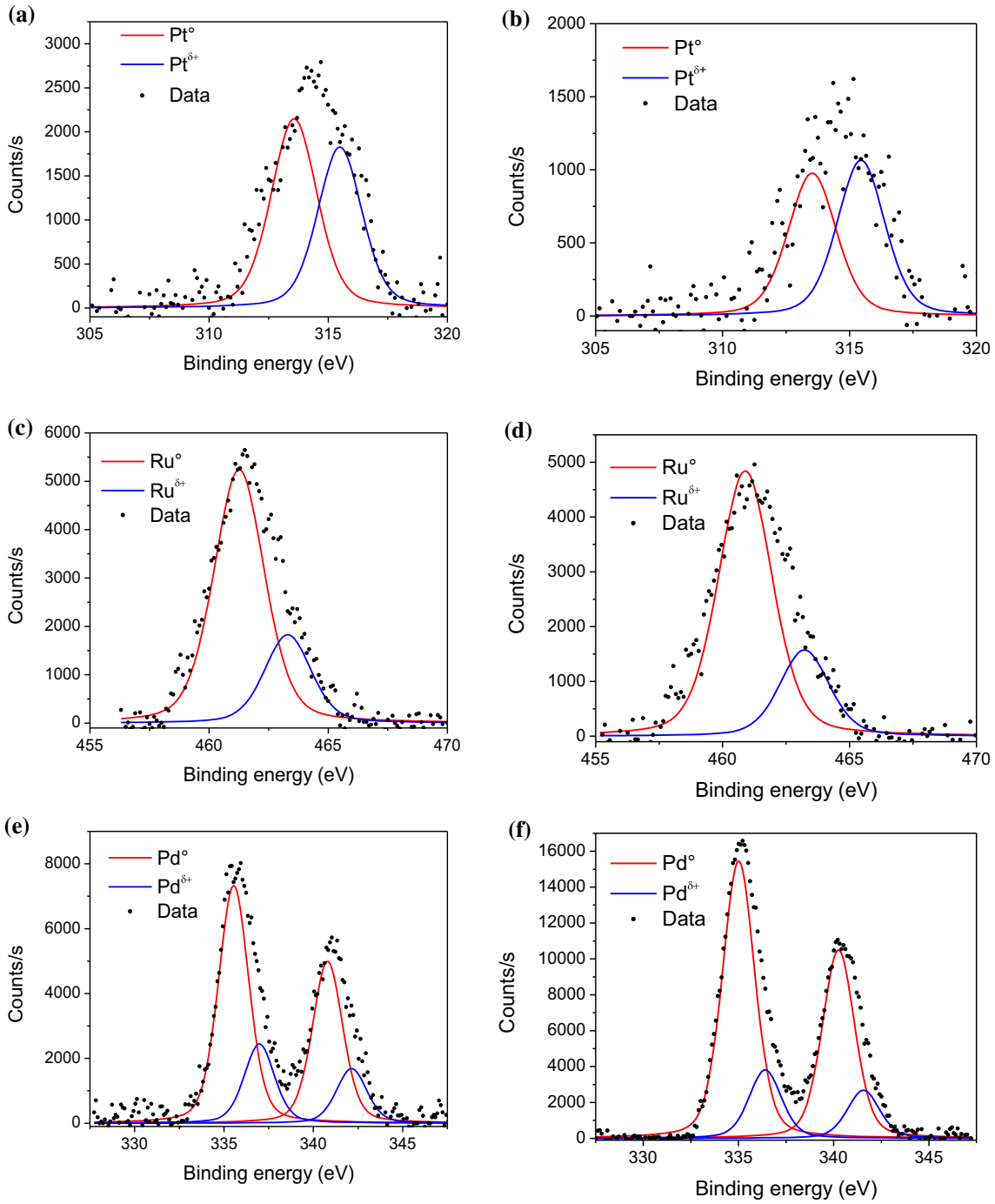

Fig. 7 Metal species distribution in catalysts as determined by XPS. **a** 1Pt-BTAl, **b** 1Pt-UTAl, **c** 1Pd-BTAl, **d** 1Pd-UTAl, **e** 1Pd-BTAl, **f** 1Pd-UTAl

- The high affinity of AC for the IPA solvent that precludes the adsorption of AC, first step for the consecutive hydrogenation to the diol (Nakamura et al. 1996).
- Because of electronic effects, the desorption of acetoin (with one π bond in its structure) would be favored while in the reaction medium enough 2,3-butanedione (2 π bonds) were present.
- The presence of an egg-shell metal distribution, that favors a rapid desorption of the intermediate product, 3-hydroxy-2-butanone, thus decreasing the possibility of over hydrogenation to 2,3-butanediol (Carrara et al. 2014). This is a known result for systems of consecutive reactions under diffusive or chemical control.

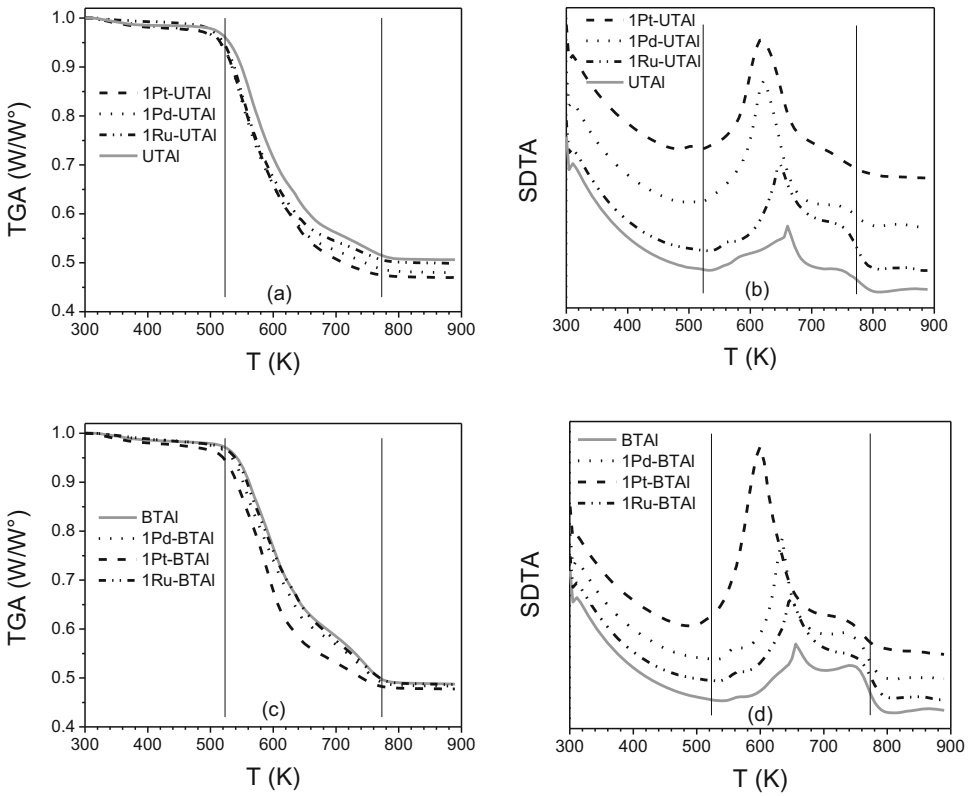

Fig. 8 Thermogravimetry results. **a** TGA of UTAl support and catalysts, **b** SDTA of UTAL support and catalysts, **c** TGA of BTAl support and catalysts, **d** SDTA of BTAL support and catalysts

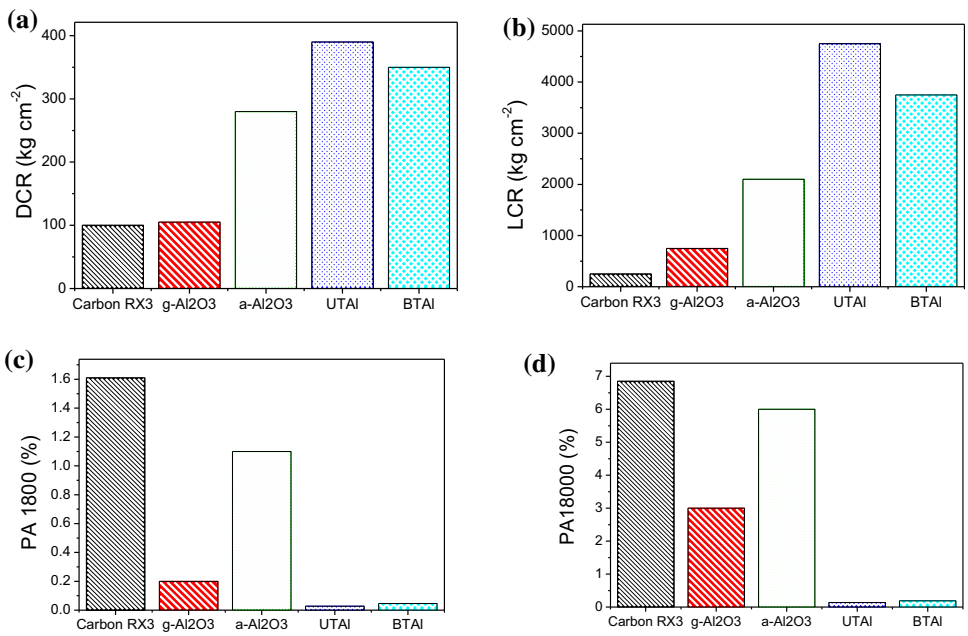

Fig. 9 Mechanical properties of commercial and composite supports. **a** Diametral compression resistance (DCR). **b** Longitudinal compression resistance (LCR). **c** Mass loss by attrition at 1800 turns. **d** Mass loss by attrition at 18,000 turns

Analysis of the effect of the type of metal used, kind of support and chloride is now presented:

Effect of the type of metal

As stated in the "Experimental" section, a solution of HCl was used to reach pH 1 in the case of the precursors $PdCl_2$, $RuCl_3$ and H_2PtCl_6, so the stabilized species at this pH are the tetrahedral complexes $[PdCl_4]^{2-}$ and $[RuCl_4]^{-}$,and octahedral $[PtCl_6]^{2-}$. All of these complexes are electron donor Lewis bases (Greenwood and Earnshaw 1997) and it is expected than during impregnation they get chemisorbed on the basic sites (Lewis sites) of alumina. In the case of composite supports the interaction between the metal and

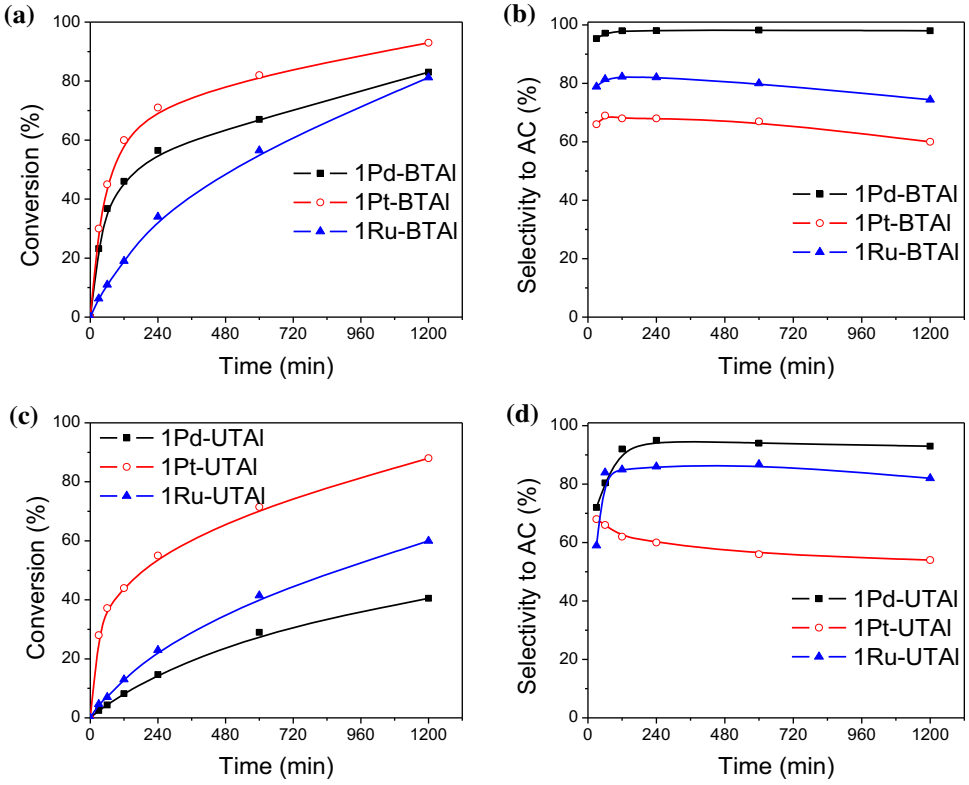

Fig. 10 Catalytic test results. Pd, Pt and Ru catalysts. **a** Conversion as a function of time, BTAl catalysts. **b** Selectivity to AC, BTAl catalysts. **c** Conversion as a function of time, UTAl catalysts. **d** Selectivity to AC, UTAl catalysts

Table 2 Values of conversion and selectivity to acetoin at selected values of reaction time, and turnover frequency

Catalyst	X_{DC} (%) $t = 60$ min	S_{AC} (%) $t = 60$ min	X_{DC} (%) $t = 120$ min	S_{AC} (%) $t = 120$ min	TOF (s^{-1}) × 10^{-2}
1Pt-BTAl	45.12	69.80	60.33	68.64	7.90
1Pt-UTAl	37.22	66.31	44.12	62.08	6.29
1Ru-BTAl	11.05	81.45	19.35	82.32	1.80
1Ru-UTAl	7.09	83.94	13.06	85.12	1.08
1Pd-BTAl	36.79	97.15	46.04	98.10	11.48
1Pd-UTAl	4.34	80.41	8.18	94.50	1.21

Experimental conditions: $V_{IPA} = 60$ mL, $C°_{DC} = 0.188$ M, $T = 353$ K, $P_{H2} = 20$ bar, $W_{CAT} = 500$ mg

the support surface is a consequence of dispersion forces (Cagnola et al. 2012). Shape and the size of the molecules affect the magnitude of the dispersion forces between them. Larger and heavier atoms and molecules exhibit stronger dispersion forces than smaller and lighter ones, so the dispersion forces are proportional to the size of the ion. In our case taking into account the sizes of these complexes the dispersion forces order would be: $[PtCl_6]^{2-}$ - $[RuCl_4]^{-} > [PdCl_4]^{2-}$. As the shape of the platinum precursor complex is octahedral, quite bigger size than the tetrahedral palladium or ruthenium complexes, this species would have higher dispersion. On the composite support there would be geometrical effects causing the highest dispersions of Pt-BTAl and Pt-UTAl.

Two active sites were detected by XPS, Me° and $Me^{\delta+}$. The results seem to indicate that both are necessary during the hydrogenation of DC:

(a) Me° sites: during hydrogenation reactions, metallic centers rich in electrons can cleave the hydrogen bond by means of the interaction of a filled *d* metal orbital (HOMO) with the empty sigma antibonding molecular orbital of H_2 (LUMO) (Shriver et al. 1994). The rupture of the hydrogen bond is more easily done on metals with a high amount of available electrons in the external *d* orbital, as it is the case of palladium (d^{10}). This rupture should be less likely on metals with fewer *d* electrons, as in the case of Pt (d^9) or Ru (d^8) (Badano et al. 2010b). Therefore, the differences in activity during the hydrogenation of DC between the

composite catalysts could be partly attributed to differences in the electronic density of the external *d* orbital of each metal that promotes the dissociative chemisorption of hydrogen.

(b) Me^{n+} sites: these species are necessary as Lewis acid sites to chemisorb diacetyl, a Lewis base. The lowest activity shown by Pd-UTAl could be explained by an electronic effect because Pd-UTAl had the lowest amount of electrodeficient Pd^{n+} species.

In a previous work of our group (Carrara et al. 2014) it was proved that during the hydrogenation of 2,3-butanedione the reaction kinetics could be explained by a Horiuti–Polanyi mechanism in which the addition of an H atom to the carbonyl group in the adsorbed state is the rate limiting step. The lower selectivity to AC of the Pt-composite or the Ru-composite catalysts could be related to the small particle size of the metal function in these materials. This would promote the overhydrogenation of DC.

Effect of the support

When comparing the results of the metals supported over BTAl in comparison to the same metal supported over UTAl it is seen in all cases that the total conversion of DC and the selectivity to acetoin are higher for the BTAl catalysts. This result was also previously found when comparing composite-supported Pd catalysts of different metal loading for the hydrogenation of styrene, 1-heptyne or 3-hexyne (Badano et al. 2010a; Carrara et al. 2015).

The difference in activity could be due to the presence of different groups, specifically basic Lewis sites that remain on the surface of the support after the polymerization step of the support preparation procedure. These would be amide groups in the case of UTAl and aromatic groups in the case of BTAl. Lewis sites would generate electronic and geometric effects that in turn would favor the formation of metal species of different electronic density. Metal particles under this interaction could reach different final sizes. This interaction could also be responsible for the lower concentration of surface chlorine over the UTAl support.

Effect of the chloride

Chloride had a clear influence in enhancing the activity of the composite catalysts. Chloride ions would stabilize electropositive M^{n+} surface atoms. Metal atoms bearing a partial positive charge would form bonds with the CO groups of diacetyl and would be important both for adsorption and hydrogenation. From the classical Blyholder model for CO interaction with transition metal surface atoms, electronic depletion of the **d** band would leave empty orbitals available for accommodating **5σ** electrons from the carbonyl group, forming new **σ** bonding and antibonding orbital fragments. In the synthetized catalysts, the chloride ions are those of the metal precursors that remain on the catalysts, after the thermal treatments performed. The fraction of electropositive M^{n+} was higher in almost all Me-BTAl catalysts (25, 24 and 45% for Pd, Ru and Pt, see Table 1) as compared to the Me-UTAl ones (20, 23 and 52 for Pd, Ru and Pt). The BTAl catalysts had the highest activity of metal catalyst series. A clear pattern of relative higher activity for those materials with higher Cl^- content can be found that stabilize electropositive M^{n+} sites, where diacetyl is chemisorbed.

Regarding the selectivity, the pattern is not clear because Pd and Pt catalysts with lower chloride content were, respectively, the highest and the least selective to acetoin. The lower selectivity to AC of Pt-composite catalysts could be related to the higher fraction of electrodeficient Pt^{n+}, ca. 50%, that favors overhydrogenation.

Conclusions

Two composite supports were used to prepare different Pt-, Pd- and Ru-supported noble metal catalysts. The effects of the type of metal and the type of composite support on the activity and selectivity during the hydrogenation of 2,3-butanedione were studied. The catalysts were characterized by ICP, XRD, OM, TEM, EPMA, XPS, TGA and mechanical resistance tests.

An egg-shell metal distribution was observed by OM and EPMA. TEM allowed to distinguish the Pt, Ru and Pd metal phases surrounding the alumina phase. OM, EPMA and TEM micrographs confirmed that the metal deposition mechanism is related to the dual hydrophilic–hydrophobic action of the alumina–polymer matrix. The acidic aqueous solution of the metal precursor would wet the hydrophilic particles (alumina) located more near the external surface while the hydrophobic polymeric material would act as a barrier preventing the impregnation of the inner particle core. Different dispersion forces of the precursor complex metals would lead to different particle sizes on the surface, the order being Pt < Ru < Pd.

XPS results indicated that the composite-supported metal particles have both Me° and $Me^{\delta+}$. after the high-temperature treatment in hydrogen. These species would be important necessary sites collaborating during the hydrogenation reactions. It was rationalized that the hydrogen bond cleavage is performed on the totally reduced Me° active sites while the substrate adsorption occurs on the electron-deficient $Me^{\delta+}$ site. The synergism between these sites for undertaking a selective hydrogenation transformation seems not to have been reported before.

The prepared composite-supported noble metal catalysts were found to be active and selective for the hydrogenation of 2,3-butanedione. The following order of activity was obtained: Pd > Pt > Ru. The differences in activity during the hydrogenation of DC between the composite catalysts could be partly attributed to differences in the electronic density of the external *d* orbital of each metal that promotes the dissociative chemisorption of hydrogen. This cleavage is more easily performed on the metal with the highest amount of electrons in the external *d* orbital (Pd) and more difficultly on the metal with the smallest number of *d* electrons (Ru).

Palladium, platinum and ruthenium catalysts with low metal loading displayed high selectivity values (>75%), the order of selectivity to AC being Pd > Ru > Pt. The high selectivity to the intermediate product could be partly related to the preferential location of the metal particles near the catalyst surface. Diffusion into long pores could lead to overhydrogenation of DC.

Higher values of catalytic activity and selectivity to AC were got when supporting the metal over the BTAl support. These results could be related to a different surface concentration of basic Lewis sites remaining after the polymerization step. The basic groups would be amides in the case of the UTAl support and aromatic nuclei in the case of BTAl. These groups would interact with the metal precursor species during impregnation and would influence the final distribution of metal particle sizes. After reducing at 503 K different metal species will be present and different chlorine levels.

The most active and selective catalyst was Pd-BTAl related to electronic effects of both palladium and the support.

Composite BTAl and UTAl supports proved to have excellent mechanical properties, even better than those of commercial γ-Al_2O_3, α-Al_2O_3 and carbon. Both supports displayed a higher resistance to diametral and longitudinal compression and to attrition. The improved properties were attributed to the intimate contact between the organic and inorganic phase. According to the MO and TEM images the polymer phase surrounds the alumina particles and increases their resistance.

Acknowledgements We thank CONICET, ANPCyT and UNL for the financial assistance of this work (Grants PIP 112-201101-00410 and 112-201301-00457, PICT and CAI + D).

References

Andrzejewska E, Kusch P, Andrzejewski M (1993) Thermal decomposition of crosslinked polymers of some dimethacrylate esters. Polym Degrad Stab 40:27–30

Augustine RL (1997) Selective heterogeneously catalyzed hydrogenations. Catal Today 37:419–440

Badano JM, Betti C, Rintoul I, Vich-Berlanga J, Cagnola E, Torres G, Vera C, Yori J, Quiroga M (2010a) New composite materials as support for selective hydrogenation; egg-shell catalysts. Appl Catal A 390:166–174. doi:10.1016/j.apcata.2010.10.008

Badano JM, Quiroga M, Betti C, Vera C, Canavese S, Coloma-Pascual F (2010b) Resistance to sulfur and oxygenated compounds of supported Pd, Pt, Rh, Ru catalysts. Catal Lett 137:35–44. doi:10.1007/s10562-010-0336-x

Cagnola E, Liprandi D, Paredes J, Badano JM, Quiroga M (2012) A high (Z)/(E) ratio obtained during the 3-hexyne hydrogenation with a catalyst based on a Rh(I) complex anchored on a carbonaceous support. Catal Lett 142:231–237

Carrara N, Badano JM, Torres G, Bertero N, Betti C, Martinez-Bovier L, Quiroga M, Vera C (2014) Kinetics of the liquid phase selective hydrogenation of 2,3-butanedione over new composite supported Pd catalysts. J Chem Technol Biotechnol 89(2):265–275. doi:10.1002/jctb.4113

Carrara N, Badano JM, Betti C, Lederhos C, Rintoul I, Coloma-Pascual F, Vera C, Quiroga M (2015) Selective hydrogenation by novel composite supported Pd egg-shell catalysts. Catal Commun 61:72–77. doi:10.1016/j.catcom.2014.12.012

Di Vona ML, Floris B, Luchetti L, Rosnati V (1990) Single electron transfers in zinc-promoted reactions. The mechanisms of the clemmensen reduction and related reactions. Tetrahedron Lett 31:6081–6084

Gertosio V, Santini CC, Basset JM, Buendia J, Vivat M (1999) Heterogeneous chemo-, regio- and diastereoselective hydrogenation of steroidic alpha-diketone. J Mol Catal A Chem 142:141–145

Grafje H, Kornig W, Weitz H, Reib W, Steffan G, Diehl H, Bosche H, Schneider K, Kieczka H (2012) Butanediols, butenediol, and butynediol. In: Wiley-VCH Verlag GmbH & Co. KGaA W (ed) Ullman's encyclopedia of industrial chemistry, vol 6, pp 407–415

Greenwood NN, Earnshaw A (1997) Chemistry of the elements, 2nd edn. Butterworth-Heinemann, Leeds

Hayakawa R, Sahara T, Shimizu M (2000) Reduction of 1,2-diketones with titanium tetraiodide: a simple approach to a -hydroxy ketones. Tetrahedron Lett 41:7939–7942

Huang SY, Chang SM, Yeh CT (2006) Characterization of surface composition of platinum and ruthenium nanoalloys dispersed on active carbon. J Phys Chem B 110:234–239. doi:10.1021/jp054870k

Huang S, Zhang C, He H (2008) Complete oxidation of o-xylene over Pd/Al2O3 catalyst at low temperatura. Catal Today 139:15–23

Iglesia E, Soled S, Baumgartner JE, Reyes S (1995) Synthesis and catalytic properties of eggshell cobalt catalysts for the Fisher–Tropsch synthesis. J Catal 153:108–122

La surface (2016) In: La Surf. Database. XPS X-Ray photoelectron spectroscopy. Roland Benoit CNRS Orléans. http://www.lasurface.com

Lin T, Chou T (1994) Selective hydrogenation of isoprene on eggshell and uniform palladium profile catalysts. Appl Catal A 108:7–19

Marshall R, Webb G, Jackson SD, Lennon D (2005) Propyne hydrogenation: characteristics of a carbon-supported palladium catalyst that exhibits a kinetic discontinuity effect. J Mol Catal A Chem 226:227–230

Nakamura K, Kondo S, Kawai Y, Hida K, Kitano K, Ohno A (1996) Enantio- and regioselective reduction of alfa-diketones by Baker's yeast. Tetrahedron Asymmetry 7:409–412

Ngamsom B, Bogdanchikova N, Borja MA, Praserthdam P (2004) Characterisations of Pd-Ag/Al_2O_3 catalysts for selective acetylene hydrogenation: effect of pretreatment with NO and N_2O. Catal Commun 5:243–248

NIST National Institute of Standarts and Technology (2016) In: X-ray photoelectron spectroscopy. Database NIST Stand. Ref.

Database 20, Version 3.5. National Institute of Standards and Technology (NIST), USA. https://srdata.nist.gov/xps

Onoe T, Iwamoto S, Inoue M (2007) Synthesis and activity of the Pt catalyst supported on CNT. Catal Commun 8:701–706

Osawa T, Harada T, Takayasu O (2000) Progress of enantio-differentiating hydrogenation of prochiral ketones over asymmetrically modified nickel catalysts and a newly proposed enantio-differentiation model. Top Catal 13:155–168

Parent YO, Magrini K, Landin SM, Ritland MA (2011) Attrition resistant fluidizable reforming catalyst. United States Patent US 7,915,196 B2

Rylander PN (1985) Hydrogenation methods. Academic Press, London

Scherzer J (1991) Attrition resistant cracking catalyst. United States Patent US 4,987,110

Serrano-Ruiz JC, Huber GW, Sánchez-Castillo MA, Dumesic JA, Rodríguez-Reinoso F, Sepúlveda-Escribano A (2006) Effect of Sn addition to Pt/CeO_2–Al_2O_3 and Pt/Al_2O_3 catalysts: an XPS, ^{119}Sn Mössbauer and microcalorimetry study. J Catal 241(2):378–388

Shriver DF, Atkins PW, Langford CH (1994) Inorganic chemistry, 3rd edn. WH Freeman and Co., New York

Shul YG, Sugiura T, Tatsumi T, Tominaga H (1986) Durability of zeolite supported RusinglebondPt bimetallic catalysts for isoalkane synthesis from synthesis gas. Appl Catal 24:131–143

Toukoniitty E, Kuusisto J, Nieminen V, Hotokka M, Salmi T (2003) Solvent effects in enantioselective hydrogenation of 1-phenyl-1,2-propanedione. J Mol Catal A Chem 192:135–151

Zuo X, Li Y, Liu H (2001) Modification effect of metal cations on the stereoselective hydrogenation of 2, 3-butanedione. Catal Lett 71:177–180